

# A model of a pumped continuous atom laser

Nicholas Robins<sup>1</sup>, Craig Savage<sup>1</sup>, and Elena Ostrovskaya<sup>2</sup>

<sup>1</sup> Department of Physics, Australian National University, ACT 0200, Australia

<sup>2</sup> Optical Sciences Centre, Australian National University, ACT 0200, Australia

## 1 Introduction

At the end of the millennium a continuous wave (cw) pumped atom laser remains to be experimentally demonstrated. The prototype atom lasers that have been operated have used rapidly pulsed or continuous output coupling, but lacked pumping of the trapped atom laser mode [1,2], as is needed for a cw laser system. Indeed, apart from simple rate equation descriptions, existing theoretical models do not incorporate both pumping of the laser mode and propagation of the out-coupled beam.

We have used the macroscopic wave-function approximation, or mean field approximation, which leads to the Gross-Pitaevskii (GP) equation, as the basis for a complete cw atom laser model. The macroscopic wave-function is the order parameter for a Bose-Einstein condensate of atoms. Our model system is schematically illustrated in Fig. 1. It includes a pumped reservoir of un-condensed atoms irreversibly coupled to the atom laser mode [3]. The condensed atoms in this mode, and in the output beam, undergo two-body interactions and three body recombination. The atoms are reversibly coupled from the atom laser mode to the output beam by a Raman process [1,3]. We solve the resulting system of coupled differential equations numerically in one spatial dimension. The macroscopic wave-function of the output atoms is analysed to determine quantities such as linewidth. Previous work based on systems of coupled equations of the complex Ginzburg-Landau type (GP equations with gain and loss) has either neglected important physics, such as

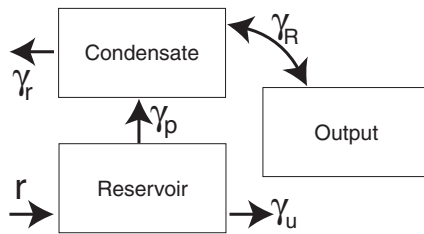


**Fig. 1.** Schematic representation of the model system. The symbols stand for the coupling, pumping and loss rates and are defined in the text.

the pumping [4,5] or has concentrated solely on the condensate, ignoring the spatio-temporal structure of the output atom beam [6].

## 2 The model

We consider the trapped atom laser mode, which we refer to as the “laser mode”, to be a one-dimensional condensate in a highly anisotropic, cigar-shaped harmonic trapping potential. The atoms in the laser mode and in the output beam are described by the macroscopic wave-functions  $\Psi_a(x, t)$  and  $\Psi_b(x, t)$  respectively. They experience two-body repulsive atom-atom interactions and three-body recombination. A novel feature of our model is the saturated loss due to the three-body recombination process [7,8].

To describe pumping we use the phenomenological model of Kneer et.al. [6] which mimics the pumping mechanism of a conventional optical laser. The number of atoms in the uncondensed pump reservoir is  $N_u(t)$ , and their spatial distribution is not modeled. The reservoir is fed at a rate  $r$ , loses atoms at the rate  $\gamma_u N_u$ , and pumps the laser mode at the rate  $\gamma_p N_u N_a$ , where  $N_a(t) = \int_{-\infty}^{\infty} |\Psi_a|^2 dx$  is the total number of atoms in the laser mode.

The laser mode is coupled, by a reversible two-photon Raman transition, to an untrapped electronic state which is the output atom laser beam  $\Psi_b(x, t)$  [1,3]. The Raman transition may also give a momentum kick to the out-coupled atoms. In an experiment the magnitude of this kick depends on the relative geometry of the two Raman laser beams. The output atom beam accelerates due to gravity. Inside the trap it overlaps, and hence interacts with, the laser mode atoms. This interaction has both a linear contribution, due to the Raman coupling, and a nonlinear contribution due to the inter-species atom-atom interactions.

Mathematically, our model is described by the following dimensionless equations:

$$\begin{aligned}
 i \frac{\partial \Psi_a}{\partial t} &= -\frac{1}{2} \frac{\partial^2 \Psi_a}{\partial x^2} + \frac{1}{2} x^2 \Psi_a + U_a \Psi_a |\Psi_a|^2 + U_{ab} \Psi_a |\Psi_b|^2 \\
 &\quad - i \gamma_r \Psi_a (|\Psi_a|^4 + |\Psi_b|^4) + \gamma_R e^{ikx} \Psi_b + \frac{i}{2} \gamma_p N_u \Psi_a, \\
 i \frac{\partial \Psi_b}{\partial t} &= -\frac{1}{2} \frac{\partial^2 \Psi_b}{\partial x^2} + Gx \Psi_b + U_b \Psi_b |\Psi_b|^2 + U_{ab} \Psi_b |\Psi_a|^2 \\
 &\quad - i \gamma_r \Psi_b (|\Psi_a|^4 + |\Psi_b|^4) + \gamma_R e^{-ikx} \Psi_a, \\
 \frac{dN_u}{dt} &= r - \gamma_u N_u - \gamma_p N_u N_a,
 \end{aligned} \tag{1}$$

where  $U_a$  and  $U_b$  are the intra- and  $U_{ab}$  the inter- species two-body interaction coefficients,  $\gamma_r$  is the three-body recombination coefficient, and  $\gamma_R$  is the Raman coupling coefficient.

The model is made dimensionless using the characteristic unit of length  $l = (\hbar/\omega m)^{1/2}$  and time,  $\tau = \omega^{-1}$ , where  $\omega$  is the trap frequency in the direction of the weak confinement. We use  $\omega \approx 125$  Hz and  $m \approx 10^{-26}$  kg. The dimensionally correct [5] two-body interaction coefficients, which we assume to be equal, can be written as  $U_{a,b,ab} = 4\pi a_s/l$  where  $a_s$  is the s-wave scattering length for a specific process. There is some arbitrariness in how the  $U_{a,b,ab}$  relate to their three dimensional counterparts. The scaling we have chosen gives a realistic condensate size [5]. Similar reasoning applies to the choice of the three-body recombination rate,  $\gamma_r$ . We have set it to give feasible lifetimes for the laser mode condensate: it is typically between  $10^{-7}$  and  $10^{-9}$  in our simulations. In accordance with experimentally reasonable values, we allow the dimensionless Raman coefficient,  $\gamma_R = \Omega_1\Omega_2/(\omega\Delta)$ , to range up to  $10^4$ , where  $\Omega_{1,2}$  are the Rabi frequencies of the Raman lasers and  $\Delta$  is the laser detuning [3], and we take the dimensionless Raman momentum kick to lie in the range  $0 \leq k \leq 100$ . The dimensionless gravitational coefficient  $G = g(m\omega^{-3}\hbar^{-1})^{1/2}$  varies in the range  $0 \leq G \leq 68$ , with  $G = 68$  corresponding to  $g = 9.8$  ms $^{-2}$ . Physically, we may think of the output atomic beam propagating in a tilted atom waveguide [9], with the tilt angle determining the value of  $G$ .

### 3 Rate equations

Given the complexity of the model equations (1), a numerical method is the only feasible method of solution. However, some understanding of the dynamics of the system can be gained by deriving approximate rate equations for the populations of the reservoir, condensate and output fractions [10]. We proceed by projecting the condensate and output mean fields onto the stationary state modes  $\Phi_a(x)$  and  $\Phi_b(x)$  defined by:

$$\Psi_a(x, t) = a(t)\Phi_a(x) \quad \Psi_b(x, t) = b(t)\Phi_b(x)e^{-ikx}, \quad (2)$$

where  $\Phi_{a,b}$  satisfy the time independent, lossless, and decoupled form of the equations (1):

$$\begin{aligned} \frac{1}{2} \frac{\partial^2 \Phi_a}{\partial x^2} &= -\mu_a \Phi_a + \frac{1}{2} x^2 \Phi_a + U_a \Phi_a |\Phi_a|^2, \\ \frac{1}{2} \frac{\partial^2 \Phi_b}{\partial x^2} &= -\mu_b \Phi_b + Gx \Phi_b + U_b \Phi_b |\Phi_b|^2. \end{aligned} \quad (3)$$

We are free to choose the magnitude of the chemical potentials  $\mu_a$  and  $\mu_b$ . In order to simplify the analysis we set the momentum kick,  $k$ , equal to zero. By doing so, we neglect the main effect the momentum kick has on the dynamics of the system, that is, the change in the spatial overlap between the condensate and the out-coupled field.

The first equation in (3) describes the eigenfunction of a trap with chemical potential  $\mu_a$ . The equation for the output mode describes a falling wave

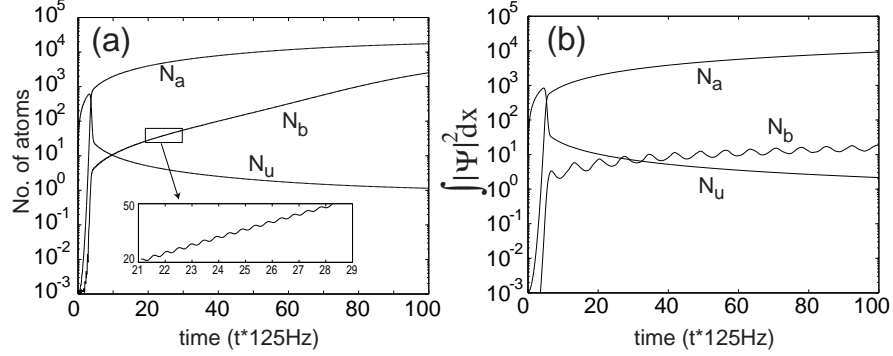


**Fig. 2.** Typical population dynamics without three-body recombination. **(a)** From the rate equations (4) showing the growth of the laser mode. We have tested that this growth continues in the long time limit ( $\tau > 600$ ). Parameters are  $r = 200$ ,  $\gamma_p = \gamma_u = 0.01$ ,  $\gamma_R = 0.5$ ,  $U_a = U_b = 0.02$ ,  $U_{ab} = 0.01$ ,  $\delta\mu = 0.02$ ,  $N_a(t=0) = 0.001$ ,  $N_b(t=0) = 10$  and  $\gamma_r = 0$ . Values of the spatial integrals are as given in the text. The inset shows the Rabi-type oscillations, present in the condensate and output fields. **(b)** From the full GP equations (1). Parameters are the same as for part (a) and  $G=68$ ,  $k=5$ . The GP simulations predict a much smaller number of atoms in the output beam,  $N_b$ , than the rate equations, because there is an effective loss of atoms due to the boundary absorber at the edge of the numerical grid.

and can be solved numerically or perturbatively, using a superposition of Airy functions in the linear limit [11]. We now substitute the ansatz (2) into the original system (1), and use the equations (3) to simplify the result. We then integrate out the spatial dependence in the equations and separate the time dependence of the modal amplitudes as  $a = n_a(t)e^{i\theta_a(t)}$  and  $b = n_b(t)e^{i\theta_b(t)}$ . By noting that the relationship between the modal amplitudes and the population numbers is given by  $N_a = I_6\delta n_a^2$  and  $N_b = I_5\delta n_b^2$ , we arrive at the following system of equations for the real population numbers  $N_{a,b}$ ,  $N_u$ , and phase difference  $\theta = \theta_b - \theta_a$ :

$$\begin{aligned}
 \frac{dN_a}{dt} &= -(\alpha N_a^3 + \beta N_a N_b^2) + \gamma_p N_u N_a + 2\gamma_R \sqrt{I_5 I_6 N_a N_b} \sin(\theta), \\
 \frac{dN_b}{dt} &= -(\beta N_b^3 + \alpha N_b N_a^2) - 2\gamma_R \sqrt{I_5 I_6 N_a N_b} \sin(\theta), \\
 \frac{d\theta}{dt} &= \delta\mu + \delta_{NL} + \frac{\gamma_R \sqrt{I_5 I_6}}{\sqrt{N_a N_b}} \cos(\theta) (N_b - N_a) \\
 \frac{dN_u}{dt} &= r - \gamma_u N_u - \gamma_p N_u N_a,
 \end{aligned} \tag{4}$$

where  $\delta\mu = (\mu_a - \mu_b)$ ,  $\alpha = (2\gamma_r I_3)/(\delta I_6)^2$ ,  $\beta = (2\gamma_r I_4)/(\delta I_5)^2$ , and  $\delta_{NL} = U_b(1 - N_b/(\delta I_5))I_2 + U_a(N_a/(\delta I_6) - 1)I_1 + U_{ab}((N_a I_1)/(\delta I_6) - (N_b I_2)/(\delta I_5))$ .

The constant coefficients  $I_s$ , where  $s = 1, 2, 3, 4, 5, 6$ , and  $\delta$  are determined by spatial overlap integrals as follows:

$$\begin{aligned}
I_1 &= \delta^{-1} \int \Phi_a \Phi_b |\Phi_a|^2 dx, & I_2 &= \delta^{-1} \int \Phi_a \Phi_b |\Phi_b|^2 dx, \\
I_3 &= \delta^{-1} \int \Phi_a \Phi_b |\Phi_a|^4 dx, & I_4 &= \delta^{-1} \int \Phi_a \Phi_b |\Phi_b|^4 dx, \\
I_5 &= \delta^{-1} \int |\Phi_b|^2 dx, & I_6 &= \delta^{-1} \int |\Phi_a|^2 dx, & \delta &= \int \Phi_a \Phi_b dx.
\end{aligned} \tag{5}$$

For realistic parameters, and using the stationary solutions of Eq. (3) we numerically calculated these integrals to have the approximate values  $\delta = 233$ ,  $I_1 = 875$ ,  $I_2 = 1.45$ ,  $I_3 = 8.39 \times 10^5$ ,  $I_4 = 2.79$ ,  $I_5 = 0.13$  and  $I_6 = 41.3$ .

From the rate equations it is seen that the populations of the condensate and the output mode undergo nonlinear Rabi-type oscillations [12] with the effective frequency determined, in part, by the strength of the interactions through  $\delta_{NL}(U_a, U_b, U_{ab})$ , and the Raman coupling  $\gamma_R$ . In the presence of pumping and without the three-body loss terms, the condensate fraction acquires a fast growing component which prevents the system from reaching a steady state defined by  $dN_{a,b}/dt = 0$ . A typical solution to the system (4) is shown in Fig. 2(a). An important feature of this regime is the unbounded growth of the laser mode in the absence of three-body recombination, which would not be the case for a realistic atom laser. This emphasises the need to include three-body recombination in atom laser models, as we do in subsequent sections. The qualitative predictions of the rate equation model are confirmed by direct integration of the system Eq. (1), with the results shown in Fig. 2(b). It is important to note that the values of the spatial integrals,  $I_s$  and  $\delta$ , play a large part in the time evolution of the rate equations.

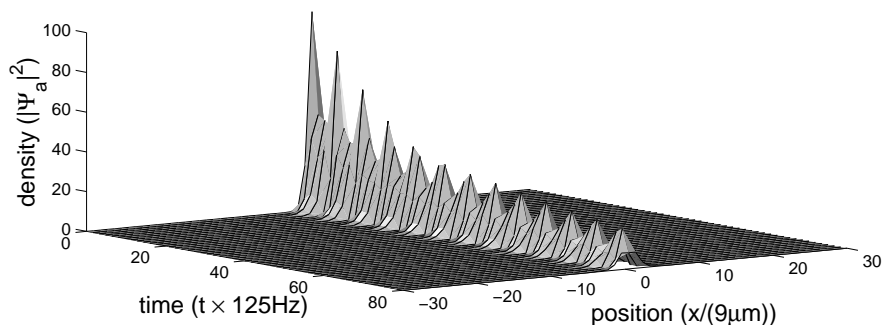


**Fig. 3.** The time evolution of an unpumped condensate. Parameters are  $\gamma_R = 0.5$ ,  $\gamma_r = 10^{-7}$ ,  $U_a = U_b = 0.02$ ,  $U_{ab} = 0.01$ ,  $G = 12$ ,  $k = 5$ , and  $N_a(t = 0) = 140$

## 4 Numerical results

With this initial understanding of the behavior of the atom laser to guide us, we proceed to investigate the numerical solution of our full model equations (1). We use a split-step method [13] to analyse the spatio-temporal behavior of the laser mode and the output beam. An absorbing boundary is used at the edges of the spatial grid. We have ensured that our results are insensitive to the size of the spatial grid and time-step.

Our model is at its simplest with the pump mechanism turned off, so that the out-coupling depletes the atom laser mode. The laser mode population changes rapidly at the beginning of the first Rabi oscillation, as can be seen in Fig.3, so the approximation of a stationary mode may be false even on short time scales [14]. One of the results of this paper is that it might be more realistic to make this approximation on the assumption of a steady state achieved through a balance of pumping and loss due to three body recombination.

We next consider the pumped system. Without the effects of gravity and interactions we find the bound state predicted by Hope et al. [15]. This is produced by the Raman coupling. A fraction of the output field remains localised around the laser mode, see Fig.4, and hence the population in the laser mode increases indefinitely due to the pumping. Hope et al. found that including gravity or two-body interactions could destroy this bound state by introducing a repulsive effective potential acting on the output mode. A large fraction of the atoms then quickly leave the interaction region. However we find that when both gravity *and* interactions act together they tend to recreate the exponentially growing output state. The population dynamics of the laser mode and the output is approximately described by Eqs.(4) in this case. The output beam's spatio-temporal structure, in the absence of three-body recombination, is shown in Fig.5.

Adding three body recombination destroys the bound state as can be seen in Fig. 6 and Fig. 7(a). This occurs because the loss rate increases as the square of the atomic density. In addition, the three-body recombination effect suppresses the atomic density noise in the output field, as well as suppressing the collective excitations of the condensate, see Fig. 7(b). Remarkably, the three body recombination process assists in creating a steady state, both in the output and laser modes, as can be seen in Fig. 7(a).

## 5 Linewidth narrowing

One of the characteristic properties of a continuous wave optical laser is the dramatic reduction in linewidth that occurs above threshold. The ultimate quantum mechanical limit to the linewidth is given by the Schawlow-Townes formula [16,17]. Graham has proposed a related limit for the atom laser due to interaction with the thermal reservoir of uncondensed atoms [18]. Our model

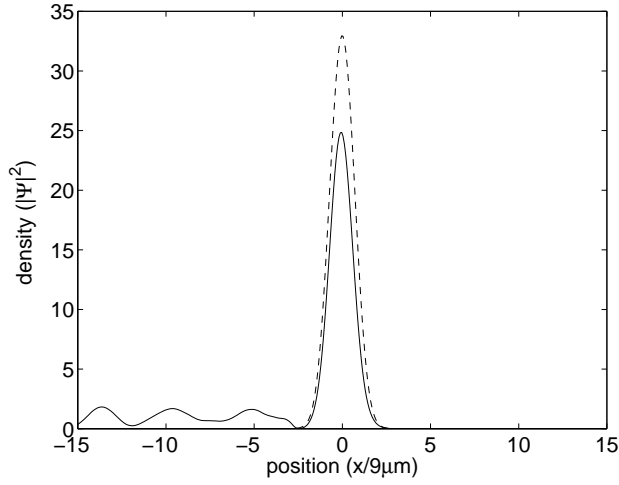


**Fig. 4.** The bound state of the laser mode (*dashed line*) and the output beam (*solid line*) at  $t = 200$ . The laser mode is multiplied by 0.003. The output beam, for  $x < -2.5$  only, is multiplied by a factor of 10. Parameters are  $r = 200$ ,  $\gamma_R = 0.5$ ,  $\gamma_r = 0$ ,  $U_a = U_b = U_{ab} = 0$ ,  $G = 0$ ,  $k = 5$ ,  $N_a(t = 0) = 0.001$ ,  $N_b(t = 0) = 10$ .

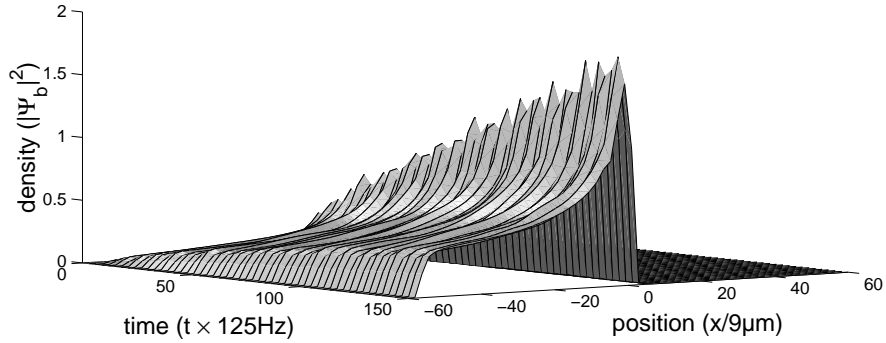


**Fig. 5.** Atom laser beam density as a function of position and time, with no three-body recombination, showing the steady growth of the output. The beam propagates in the negative  $x$  direction from the condensate centered at  $x = 0$ . Parameters are  $r = 200$ ,  $\gamma_R = 0.5$ ,  $\gamma_u = 0.1$ ,  $\gamma_p = 0.1$ ,  $\gamma_r = 0$ ,  $U_a = U_b = 0.02$ ,  $U_{ab} = 0.01$ ,  $G = 68$ ,  $k = 5$ ,  $N_a(t = 0) = 0.001$ ,  $N_b(t = 0) = 10$ .

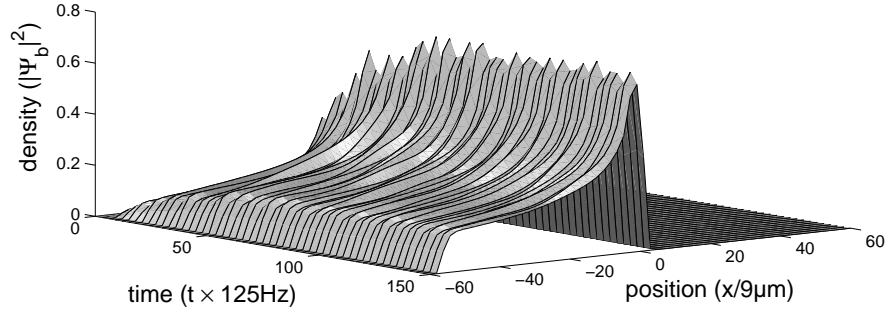


**Fig. 6.** Atom laser beam density as a function of position and time, with three-body recombination included  $\gamma_r = 10^{-7}$ , showing a quasi-steady state. Parameters are otherwise the same as for Fig. 5.

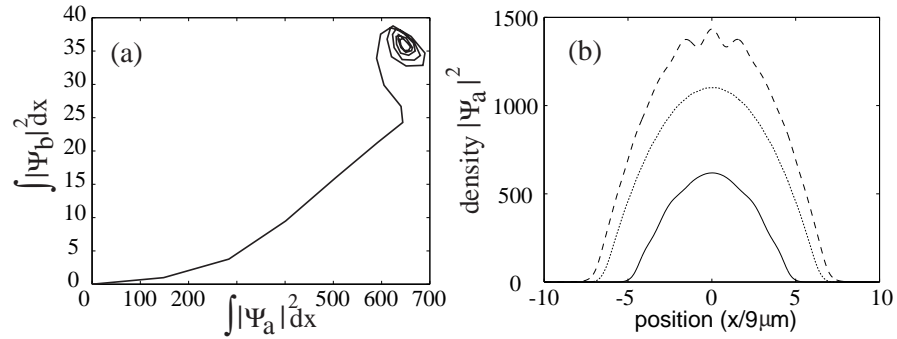


**Fig. 7.** Steady state operation of the system with three-body recombination. (a) Atom number in the output versus atom number in the laser mode. Parameters are  $r = 100$ ,  $\gamma_R = 0.5$ ,  $\gamma_u = 0.1$ ,  $\gamma_p = 0.1$ ,  $\gamma_r = 10^{-5}$ ,  $U_a = U_b = 0.02$ ,  $U_{ab} = 0.01$ ,  $G = 12$ ,  $k = 5$ ,  $N_a(t = 0) = 0.001$ ,  $N_b(t = 0) = 100$ . (b) The quasi-steady state density profile of the laser mode at  $t = 150$  for pumping of  $r = 200$  (solid) and  $r = 1600$  (dotted). Other parameters are  $\gamma_R = 0.5$ ,  $\gamma_u = 0.1$ ,  $\gamma_p = 0.1$ ,  $\gamma_r = 10^{-7}$ ,  $U_a = U_b = 0.02$ ,  $U_{ab} = 0.01$ ,  $G = 68$ ,  $k = 5$ ,  $N_a(t = 0) = 0.001$ ,  $N_b(t = 0) = 10$ . By contrast the laser mode at  $t = 150$  for pumping of  $r = 200$  (dashed), with no three-body recombination, is continuing to grow and change shape.



does not incorporate the many-body quantum physics that determines the ultimate atom laser linewidth. However, in practice we might expect that the linewidth is not determined by fundamental factors, but rather by the dynamics of the particular system; for example, in the optical case by relaxation oscillations [19]. Our model is suitable for determining the linewidth due to this type of dynamical effect.

To determine the linewidth of the output we have calculated the instantaneous spatial Fourier transforms of particular regions of the output field. The results are shown in the inset to Fig.8. The atoms are accelerated by gravity according to  $v = \sqrt{v_0^2 + 2gx}$  and hence, the velocity linewidth narrows as the atoms fall away from the trap [20]. We are currently investigating the effect of the pump rate,  $r$ , on the output linewidth of our model, in both the spatial and temporal domains.

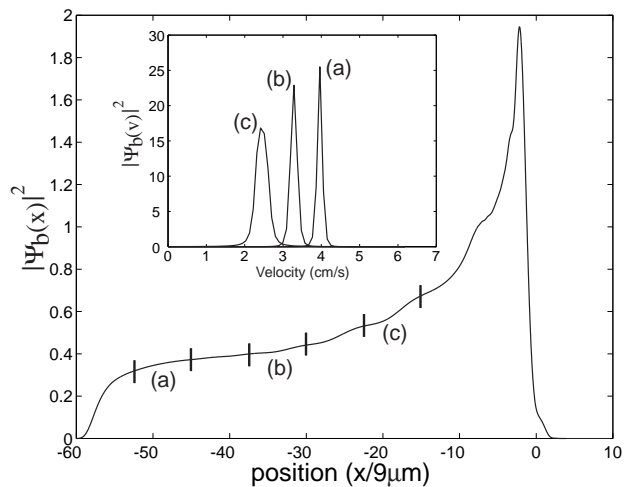


**Fig. 8.** The density of the output beam as a function of position. The inset shows the velocity linewidth over three regions of the atom laser output. These regions are labeled (a), (b), and (c) and are indicated by the bars on the main curve. Their width is about 7.5 dimensionless units, or  $68 \mu\text{m}$ . The number of atoms in each region is approximately the dimensionless density times the length; e.g.  $7.5 \times 0.4 = 3$  for region (b). Parameters are as in Fig.7(a).

## 6 Conclusion

We have presented a model of an atom laser in which we have endeavored to include the important physics of an experimental atom laser system. The resulting model exhibits a rich and complex dynamics. A novel aspect of our model is the inclusion of three-body recombination, which we believe plays an

important part in achieving steady state laser operation. We demonstrated that the complex interplay of effects in our model can lead to a steady output with low atomic density fluctuations. The output of our atom laser is locally monochromatic, its linewidth dominated by gravitational acceleration. We are in the process of generalising this one dimensional model to three dimensions.

We acknowledge continuing discussions with J. Hope, and thank G. Moy for his input.

## References

1. E. W. Hagley, L. Deng, M. Kozuma, J. Wen, K. Helmerson, S. L. Rolston, W. D. Phillips: *Science* **283**, 1706 (1999)
2. I. Bloch, T. W. Hansch, T. Esslinger: *Phys. Rev. Lett.* **82**, 3008 (1999)
3. G. M. Moy, J. J. Hope, C. M. Savage: *Phys. Rev. A* **55**, 3631 (1997)
4. J. Schneider and A. Schenzle: *App. Phys. B* **69**, 353 (1999)
5. M. Edwards, D. A. Griggs, P. L. Holman, C. W. Clark, S. L. Rolston, W. D. Phillips: *J. Phys. B: At. Mol. Opt. Phys.* **32**, 2935 (1999)
6. B. Kneer, T. Wong, K. Vogel, W. P. Shleich, D. F. Walls: *Phys. Rev. A* **58**, 4841 (1998)
7. Yu. Kagan, A. E. Muryshev, G. V. Shlyapnikov: *Phys. Rev. Lett.* **81**, 933 (1998)
8. E.A. Burt, R.W. Ghrist, C.J. Myatt, M.J. Holland, E.A. Cornell, C.E. Wieman: *Phys. Rev. Lett.* **79**, 337 (1997)
9. S. Marksteiner, C.M. Savage, P. Zoller, S.L. Rolston: *Phys. Rev. A* **50**, 2680 (1994)
10. N. Robins: Honours Thesis, Australian National University (2000)
11. J. Schneider and A. Schenzle: *App. Phys. B* **69**, 353 (1999)
12. R. J. Ballagh, K. Burnett, T. F. Scott: *Phys. Rev. Lett.* **78**, 1607 (1997)
13. T.R. Taha, M.J. Ablowitz: *J. Comp. Phys.* **55**, 203 (1984)
14. M. Naraschewski, A. Schenzle, H. Wallis: *Phys. Rev. A* **56**, 603 (1997)
15. J. J. Hope, G. M. Moy, M. J. Collett, C. M. Savage: cond-mat/9907023, *Phys. Rev. A* **61**, 023603 (2000)
16. A.L. Schawlow, C.H. Townes: *Phys. Rev.* **112**, 1940 (1958)
17. H.M. Wiseman: *Phys. Rev. A* **60**, 4083 (1999)
18. R. Graham: *Phys. Rev. Lett.* **81**, 5262 (1998)
19. A.E. Siegman: *Lasers* (University Science Books, Mill Valley 1986)
20. H.M. Wiseman: *Phys. Rev. A* **56**, 2068 (1997)